Research Article | Vol. 9, No. 3 | 1 Mar 2018 | BIOMEDICAL OPTICS EXPRESS 1272
Biomedical Optics EXPRESS

Change in human lens dimensions, lens refractive index distribution and ciliary body ring diameter with accommodation

Adnan Khan,[1,2,3] James M. Pope,[2,4] Pavan K. Verkicharla,[2,3,5] Marwan Suheimat,[2,3] and David A. Atchison[2,3,*]

[1]*Weill Cornell Medicine-Qatar, Education City, Qatar Foundation, Doha, Qatar and New York, USA*
[2]*Institute of Health & Biomedical Innovation, Queensland University of Technology, Kelvin Grove, QLD, Australia*
[3]*School of Optometry & Vision Science, Queensland University of Technology, Kelvin Grove, QLD, Australia*
[4]*School of Chemistry, Physics & Mechanical Engineering, Queensland University of Technology, Brisbane, QLD, Australia*
[5]*Brien Holden Institute of Optometry and Vision Sciences, L V Prasad Eye Institute, Kallam Anji Reddy Campus, Hyderabad, India*
[*]*d.atchison@qut.edu.au*

Abstract: We investigated changes in ciliary body ring diameter, lens dimensions and lens refractive index distributions with accommodation in young adults. A 3T clinical magnetic resonance imaging scanner imaged right eyes of 38 18-29 year old participants using a multiple spin echo sequence to determine accommodation-induced changes along lens axial and equatorial directions. Accommodation stimuli were approximately 1 D and 5 D. With accommodation, ciliary body ring diameter, and equatorial lens diameter decreased (–0.43 ± 0.31 mm and –0.30 ± 0.23 mm, respectively), and axial lens thickness increased (+ 0.34 ± 0.16 mm). Lens shape changes cause redistribution of the lens internal structure, leading to change in refractive index distribution profiles. With accommodation, in the axial direction refractive index profiles became flatter in the center and steeper near the periphery of the lens, while in the equatorial direction they became steeper in the center and flatter in the periphery. The results suggest that the anatomical accuracy of lens optical models can be improved by accounting for changes in the refractive index profile during accommodation.

OCIS codes: (170.3890) Medical optics instrumentation; (330.4875) Optics of physiological systems; (330.7322) Visual optics, accommodation.

References and links

1. M. Dubbelman and G. L. Van der Heijde, "The shape of the aging human lens: curvature, equivalent refractive index and the lens paradox," Vision Res. **41**(14), 1867–1877 (2001).
2. M. Dubbelman, G. L. Van der Heijde, and H. A. Weeber, "Change in shape of the aging human crystalline lens with accommodation," Vision Res. **45**(1), 117–132 (2005).
3. L. Ostrin, S. Kasthurirangan, D. Win-Hall, and A. Glasser, "Simultaneous measurements of refraction and A-scan biometry during accommodation in humans," Optom. Vis. Sci. **83**(9), 657–665 (2006).
4. S. A. Strenk, L. M. Strenk, J. L. Semmlow, and J. K. DeMarco, "Magnetic resonance imaging study of the effects of age and accommodation on the human lens cross-sectional area," Invest. Ophthalmol. Vis. Sci. **45**(2), 539–545 (2004).
5. A. L. Sheppard, C. J. Evans, K. D. Singh, J. S. Wolffsohn, M. C. Dunne, and L. N. Davies, "Three-dimensional magnetic resonance imaging of the phakic crystalline lens during accommodation," Invest. Ophthalmol. Vis. Sci. **52**(6), 3689–3697 (2011).
6. E. Martinez-Enriquez, P. Pérez-Merino, M. Velasco-Ocana, and S. Marcos, "OCT-based full crystalline lens shape change during accommodation in vivo," Biomed. Opt. Express **8**(2), 918–933 (2017).
7. E. A. Hermans, P. J. Pouwels, M. Dubbelman, J. P. A. Kuijer, R. G. L. van der Heijde, and R. M. Heethaar, "Constant volume of the human lens and decrease in surface area of the capsular bag during accommodation: an MRI and Scheimpflug study," Invest. Ophthalmol. Vis. Sci. **50**(1), 281–289 (2009).

#314771 https://doi.org/10.1364/BOE.9.001272
Journal © 2018 Received 4 Dec 2017; revised 14 Jan 2018; accepted 25 Jan 2018; published 21 Feb 2018

Biomedical Optics EXPRESS

8. S. Kasthurirangan, E. L. Markwell, D. A. Atchison, and J. M. Pope, "In vivo study of changes in refractive index distribution in the human crystalline lens with age and accommodation," Invest. Ophthalmol. Vis. Sci. **49**(6), 2531–2540 (2008).
9. A. Gullstrand, "The mechanism of accommodation," in *Appendix IV, Helmholtz's treatise on Physiological Optics,* 3rd ed., J. P. C. Southall, ed. (Optical Society of America, New York, 1924), pp. 382–415.
10. C. E. Jones, D. A. Atchison, and J. M. Pope, "Changes in lens dimensions and refractive index with age and accommodation," Optom. Vis. Sci. **84**(10), 990–995 (2007).
11. P. K. Verkicharla, M. Suheimat, J. M. Pope, F. Sepehrband, A. Mathur, K. L. Schmid, and D. A. Atchison, "Validation of a partial coherence interferometry method for estimating retinal shape," Biomed. Opt. Express **6**(9), 3235–3247 (2015).
12. C. E. Jones and J. M. Pope, "Measuring optical properties of an eye lens using magnetic resonance imaging," Magn. Reson. Imaging **22**(2), 211–220 (2004).
13. J. M. Adnan, J. M. Pope, F. Sepehrband, M. Suheimat, P. K. Verkicharla, S. Kasthurirangan, and D. A. Atchison, "Lens shape and refractive index distribution in type 1 diabetes," Invest. Ophthalmol. Vis. Sci. **56**(8), 4759–4766 (2015).
14. S. A. Strenk, J. L. Semmlow, L. M. Strenk, P. Munoz, J. Gronlund-Jacob, and J. K. DeMarco, "Age-related changes in human ciliary muscle and lens: a magnetic resonance imaging study," Invest. Ophthalmol. Vis. Sci. **40**(6), 1162–1169 (1999).
15. S. Kasthurirangan, E. L. Markwell, D. A. Atchison, and J. M. Pope, "MRI study of the changes in crystalline lens shape with accommodation and aging in humans," J. Vis. **11**(3), 19 (2011).
16. K. Richdale, L. T. Sinnott, M. A. Bullimore, P. A. Wassenaar, P. Schmalbrock, C.-Y. Kao, S. Patz, D. O. Mutti, A. Glasser, and K. Zadnik, "Quantification of age-related and per diopter accommodative changes of the lens and ciliary muscle in the emmetropic human eye," Invest. Ophthalmol. Vis. Sci. **54**(2), 1095–1105 (2013).
17. K. Richdale, M. A. Bullimore, L. T. Sinnott, and K. Zadnik, "The effect of age, accommodation and refractive error on the adult human eye," Optom. Vis. Sci. **93**(1), 3–11 (2016).
18. Y. Ni, X.-L. Liu, M.-X. Wu, Y. Lin, Y.-Y. Sun, C. He, and Y.-Z. Liu, "Objective evaluation of the changes in the crystalline lens during accommodation in young and presbyopic populations using Pentacam HR system," Int. J. Ophthalmol. **4**(6), 611–615 (2011).
19. V. Ramasubramanian and A. Glasser, "Objective measurement of accommodative biometric changes using ultrasound biomicroscopy," J. Cataract Refract. Surg. **41**(3), 511–526 (2015).
20. K. Richdale, M. A. Bullimore, and K. Zadnik, "Lens thickness with age and accommodation by optical coherence tomography," Ophthalmic Physiol. Opt. **28**(5), 441–447 (2008).
21. S. A. Strenk, L. M. Strenk, and S. Guo, "Magnetic resonance imaging of aging, accommodating, phakic, and pseudophakic ciliary muscle diameters," J. Cataract Refract. Surg. **32**(11), 1792–1798 (2006).
22. R. C. Augusteyn, A. Mohamed, D. Nankivil, P. Veerendranath, E. Arrieta, M. Taneja, F. Manns, A. Ho, and J. M. Parel, "Age-dependence of the optomechanical responses of ex vivo human lenses from India and the USA, and the force required to produce these in a lens stretcher: the similarity to in vivo disaccommodation," Vision Res. **51**(14), 1667–1678 (2011).
23. D. A. Atchison and G. Smith, *Optics of the Human Eye* (Butterworth-Heinemann, Oxford, England, 2000).
24. C. E. Jones, D. A. Atchison, R. Meder, and J. M. Pope, "Refractive index distribution and optical properties of the isolated human lens measured using magnetic resonance imaging (MRI)," Vision Res. **45**(18), 2352–2366 (2005).
25. R. Navarro and N. López-Gil, "Impact of internal curvature gradient on the power and accommodation of the crystalline lens," Optica **4**(3), 334–340 (2017).

1. Introduction

The human lens is asymmetric, with its anterior surface being flatter than the posterior surface [1]. During accommodation the lens changes its shape due to contraction of the ciliary muscle, which reduces zonular and capsular tension. It adopts a more rounded shape, with both surfaces (but particularly the anterior surface), becoming more curved. The lens reduces in diameter, and becomes thicker axially accompanied by a similar reduction in anterior chamber depth and a small reduction in vitreous depth [2, 3]. Strenk et al. reported increase in cross-sectional area of the anterior portion of the lens with accommodation [4], but others had reported small decreases in cross-sectional area with accommodation [5, 6]. Small increases [5] or no changes [6, 7] in volume with accommodation have been reported. Accompanying the changes in the external geometry of the lens is a change in the gradient refractive index distribution (GRIN) inside the lens [8]. Gullstrand referred to this as the intracapsular mechanism of accommodation [9].

The distribution of the GRIN in the accommodating lens has remained relatively unexplored. Kasthurirangan et al. used 2-dimensional magnetic resonance imaging (MRI) to model the axial and equatorial GRIN profiles of the human lens by power functions, but did

Biomedical Optics EXPRESS

not take into account the asymmetry of the lens [8]. MRI offers the advantage over other imaging techniques, such as Scheimpflug photography, ultrasound biomicroscopy and anterior segment optical coherence tomography, that images are free from optical distortions [10].

In this study we used 3-D MRI to investigate accommodation-induced changes in ciliary body ring diameter, lens dimensions and refractive index distribution of the in-vivo lens. We took into account the asymmetry of the lens shape, while imaging with a larger number of people, better resolution and signal to noise ratio than Kasthurirangan et al. [8].

2. Methods

2.1 Participants

Right eyes of 38 healthy young participants (18 – 29 years, 22.7 ± 3.0 years) with spherical equivalent refractions −1. 7 ± 2.4 D (range + 1.0 to −8.0 D) underwent MRI scans. All had < 1.5 D astigmatism. These people were part of a larger group of 60 participants [11]; thirteen participants could not be included because accommodation images were not acquired, and for nine participants some images had significant motion artifacts (three without, and six with accommodation).

The research adhered to the tenets of the Declaration of Helsinki. The experimental protocol was approved by the Queensland University of Technology and University of Queensland human ethics review boards. All participants were required to give written consent and to complete a standard questionnaire in order to exclude participants with heart pacemakers, aneurysm clips or other metallic implants (whose function might be affected by the magnetic field of the MRI system and cause local radio-frequency heating or image distortion), and to exclude those who might have metal fragments in the eye or head.

2.2 MRI – basic procedures

MRI was used to measure the lens refractive index distribution and lens dimensions using a 3.0 Tesla (Siemens Trio) clinical scanner in the Centre for Advanced Imaging at the University of Queensland, Australia.

During the MRI procedure, participants were positioned supine on the instrument table and heads were stabilized with padding. Participants were asked to focus (via an adjustable mirror mounted at 45° to vertical) on a white Maltese cross fixation target on a black background that was projected onto a translucent screen at the end of the magnet bore at approximately 0.93 m from the eye. A standard 4.0 cm (Siemens) circular receive-only surface coil was taped over the examined eye so that the target was visible through the hole in the center of the coil, as illustrated in Fig. 1 of reference 7). A thin spacer made from self-adhesive felt, glued to the surface of the coil body was used to minimize skin contact with the coil, in order to protect against localized radio-frequency heating. The non-examined eye was occluded using an eye patch. Participants were instructed to avoid head movement, focus on the fixation target and minimize blinking during data acquisition. They were advised to blink and/or close their eyes between data acquisitions to avoid eye dryness. Where refractions were outside the range ± 0.50 D, a lens was attached to the surface coil on the opposite side from the participant's eye so that the target became clear and imaging was performed. The distance of lenses from the eye was estimated to be 25 mm. The power of the lens was determined from the distance refraction, assumed to apply at 12 mm vertex distance. To stimulate approximately 5 D accommodation a more negative powered lens was put in place based on adding a −5 D power to the distance refraction at the 12 mm vertex distance, the participant was asked once again to focus on the target and the imaging protocols were repeated. The mean change in accommodation stimulus was approximately 4.5 D.

Biomedical Optics EXPRESS

2.3 MRI – imaging protocols

Following localizer scans to locate the position of the eye in the center of the field of view (FOV), multi-slice fast spin echo (FSE) images (64 mm FOV; 256 × 256 matrix; 2 mm slice thickness (no gaps); TR = 4000 ms; TE = 16 ms; echo train length 12, imaging time 128 s) were obtained in both axial and sagittal planes, giving in-plane resolution of 0.25 mm. A single slice multiple spin echo (MSE) sequence (64 mm FOV; 256 × 256 matrix; 2 mm slice thickness; TR = 2000 ms; 4 echoes: TE = 12.5/25/37.5/50 ms; imaging time 4.5 mins) was used to acquire data both for measuring lens dimensions and for calculating the refractive index distribution through the lens [8, 12]. The FSE images were used only to ensure that the single slice was placed through the symmetry axis of the lens, using the center slice from the sagittal FSE image to identify this axis.

In MRI of the eye lens, the proton transverse or spin-spin relaxation rate ($R_2 = 1/T_2$) is proportional to the concentration of macro-molecules (mainly crystallin proteins) in the lens, which in turn determines the refractive index [12]. A MSE sequence was used to map the R_2-distribution through the lens, by fitting the decay of pixel signal intensity S with echo time T_E for each image voxel in the lens to the single exponential decay equation

$$S(T_E) = S_0 e^{-R_2 T_E} \tag{1}$$

where S_0 is the signal intensity extrapolated to $T_E = 0$ (the signal corresponding to the equilibrium or steady state magnetization). The R_2 map can be transformed to a refractive index map at 589 nm equivalent wavelength of light, using the calibration equation [8, 12]

$$n = 1.3554 + 1.549 \times 10^{-3} R_2 - 6.34 \times 10^{-6} R_2^2 \tag{2}$$

where n is refractive index.

A normalized refractive index distribution can be defined along the axis and equator of the lens according to

$$n(r) = C_0 + C_p r^p \tag{3}$$

where r is the normalized distance from the lens center ($r = 0$ at the center and $r = 1$ at the periphery), C_0 is the index at the lens center, C_p is the difference in refractive index between the lens center and periphery, and the exponent p characterizes the gradient refractive index rate of change.

2.4 MRI – data processing

Image analysis was performed using custom built software written in Matlab (Mathworks, Natick, MA, version R2011). Full details of the image processing have been described elsewhere [13].

Due to motion and blinking in some participants, MSE images and hence refractive index maps suffered from artefacts. In order to improve signal to noise (S/N) and make comparisons between different subject groups, lens refractive index profiles were computed using the line of pixels closest to the lens axis or equatorial diameter, and also by averaging over a 3-pixel-wide band centered on these axes. Further details of this procedure together with typical examples of the refractive index profiles obtained for individual lenses can be found in Fig. 2 of our previous publication [13]. As MSE images had in-plane resolution of 0.25 mm and slice thickness of 2 mm, this gave an effective voxel size of 0.375 mm^3 (3 × 0.25 × 0.25 × 2).

The first axial MSE image (TE = 12.5 ms) with the best S/N and contrast was selected to determine the lens axial thickness, equatorial diameter and the ciliary body ring diameter manually using ImageJ software (developed at National Institutes of Health, available in the public domain at http://rsbweb.nih.gov/ij/index.html). The axial thickness was measured along the optical axis between the anterior and posterior edges of the lens and the equatorial

Biomedical Optics EXPRESS

diameter was measured along the equatorial diameter line between nasal and temporal edges of the lens. An anterior axial thickness was measured from the anterior edge of the lens to the center of the equatorial diameter line. Similarly, a posterior axial thickness was measured from the posterior edge to the center of the equatorial diameter line (Fig. 1). Ciliary body ring diameter was measured as the distance between innermost ciliary body tips. As the slice passes through the center of the lens in the MSE image, it produces an error in measurement of ciliary body ring diameter [14]. Therefore, a correction equation for the ciliary body ring diameter was employed:

$$D_c = \left[D_m^2 + S_2 \right]^{1/2} \tag{4}$$

where D_c is the corrected ciliary muscle diameter, D_m is the measured ciliary body ring diameter and S is the slice thickness.

To analyze refractive index data, lens dimensions were normalized to extend from 0 to + 1 for each participant. For the equatorial axis, the normalized dimension extended from −1 to + 1 and the data were folded about the optical axis to give a normalized dimension 0 to 1. A similar approach was used for the axial dimension, with the midpoint between anterior and posterior points as the reference point (red dot in Fig. 1). In addition, separate analyzes were performed for the portions anterior and posterior to the midpoint of the equatorial diameter (blue dot in Fig. 1). Group data of each dimension were fitted according to Eq. (3).

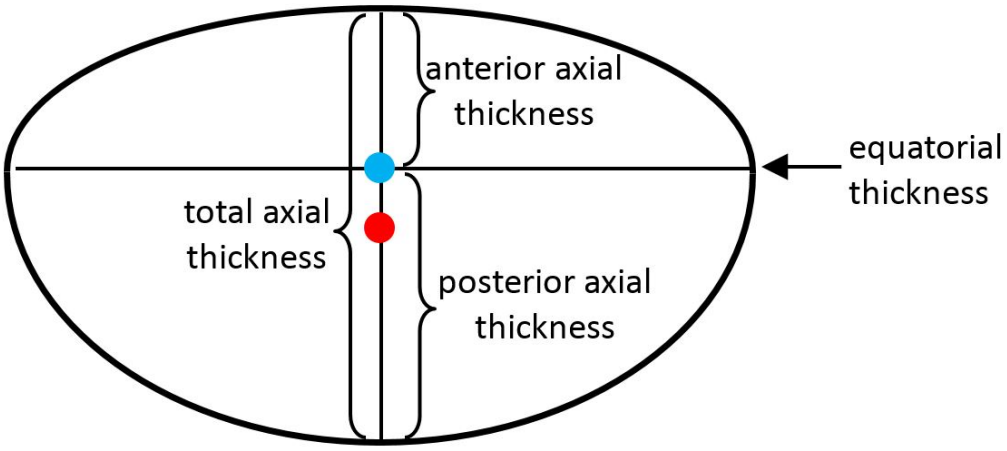

Fig. 1. Dimensions for refractive index profiles. The red dot is the axial midpoint and the blue dot is the midpoint of the equatorial diameter.

3. Results

Table 1 shows lens and ciliary ring dimensions, and Fig. 2 shows images of a typical participant without and with accommodation. All dimensions changed significantly upon accommodation. Ciliary body ring diameter and equatorial lens diameter decreased by 0.43 ± 0.31 mm and 0.30 ± 0.23 mm, respectively. Total axial lens thickness and its anterior and posterior components increased by + 0.34 ± 0.16 mm, 0.25 ± 0.25 mm and + 0.10 ± 0.18 mm, respectively. As a measure of lens shape, the ratio of the total axial lens thickness to equatorial diameter without and with accommodation was calculated (Table 1). This ratio increased with accommodation by a mean of 0.05 (13%).

Biomedical Optics EXPRESS

Table 1. Lens and ciliary ring dimensions without and with accommodation

Ocular dimension	Without accommodation mean ± SD	With accommodation mean ± SD	Difference mean ± SD	P-value paired t-test
Lens anterior axial thickness (mm)	1.29 ± 0.15	1.54 ± 0.16	0.25 ± 0.20	< 0.001
Lens posterior axial thickness (mm)	2.26 ± 0.19	2.35 ± 0.18	0.10 ± 0.18	0.002
Total axial lens thickness (mm)	3.55 ± 0.21	3.89 ± 0.21	0.34 ± 0.16	< 0.001
Lens equatorial diameter (mm)	9.29 ± 0.34	8.99 ± 0.30	–0.30 ± 0.23	< 0.001
Total axial thickness/equatorial diameter	0.38 ± 0.02	0.43 ± 0.03	0.05 ± 0.02	< 0.001
Ciliary body ring diameter (mm)	11.07 ± 0.47	10.64 ± 0.44	–0.43 ± 0.31	< 0.001

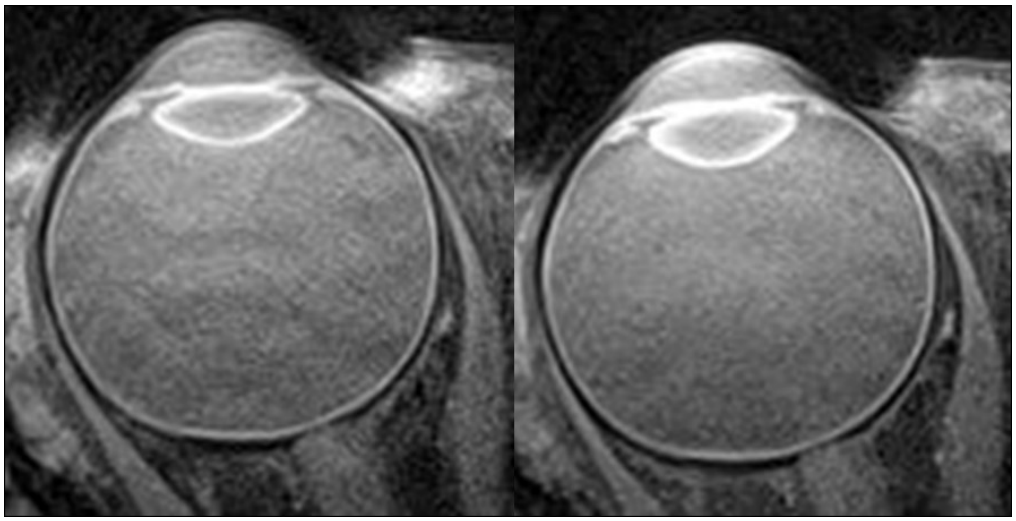

Fig. 2. Characteristic MSE images of a 21 year old male (a) without accommodation stimulus, and (b) with 5.0 D accommodation stimulus. Upon accommodation, ciliary body ring diameter and lens equatorial diameter decreased, and axial thickness increased.

The combined normalized refractive index profile data for different lens dimensions and each accommodation condition were fitted by the power Eq. (3) using Sigmaplot software. Table 2 shows the means and standard errors of the refractive index co-efficients for the anterior, posterior and total axial thicknesses, and Table 3 shows the means and standard errors of the refractive index co-efficients for the equatorial diameter. These parameters and the number of participants (38) were used to perform unpaired t-tests comparing unaccommodated and accommodated conditions using GraphPad (https://www.graphpad.com/quickcalcs/ttest1.cfm).

With accommodation, p values increased for both anterior (p = 2.14 vs p = 3.31, P = 0.03 and posterior axial segments (p = 2.79 vs p = 4.73, P = 0.04), while the equatorial p value decreased (p = 4.34 vs p = 3.66, P = 0.04). There were significant differences in C_o and C_p for the total axial thickness with accommodation, and C_o became slightly larger along the posterior axial direction (P = 0.04). C_o and C_p changed significantly along the equatorial direction (P < 0.001 and 0.04, respectively), with C_o becoming larger and C_p becoming smaller with accommodation.

Biomedical Optics EXPRESS

Table 2. Co-efficients of fit to normalized axial refractive index data. Numbers in brackets are standard errors.

Accommodation stimulus	C_o anterior	C_p anterior	p anterior	C_o posterior	C_p posterior	p posterior	C_o total axial	C_p total axial	p total axial
without accommodation	1.4026 (0.0022)	–0.0363 (0.0026)	2.1422 (0.3887)	1.4005 (0.0010)	–0.0204 (0.0017)	2.7942 (0.5597)	1.4001 (0.0008)	–0.0290 (0.0016)	3.3120 (0.3968)
with accommodation	1.4039 (0.0010)	–0.0342 (0.0015)	3.3052* (0.3687)	1.4030* (0.0007)	–0.0223 (0.0019)	4.7335* (0.7586)	1.4036* (0.0006)	– 0.0340* (0.0017)	3.3877 (0.3152)

* $P < 0.05$

Figure 3 shows the refractive index profiles of the lens anterior and posterior axial segments, plotted against normalized anterior and posterior axial distances respectively, both without and with accommodation. With accommodation, the axial refractive index profiles show increased steepness at the periphery.

Table 3. Co-efficients of fit to normalized equatorial refractive index data. Numbers in brackets are standard errors.

Accommodation stimulus	C_o	C_p	p
without accommodation	1.4012 (0.0004)	–0.0452 (0.0019)	4.3358 (0.2568)
with accommodation	1.4033* (0.0003)	–0.0366* (0.0012)	3.6612* (0.2025)

* $P < 0.05$

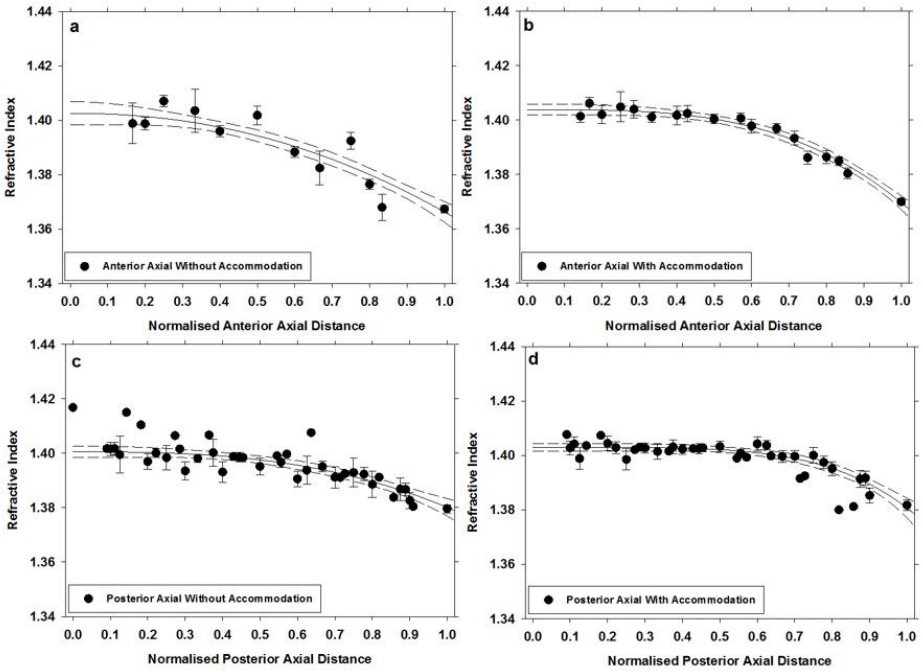

Fig. 3. Normalized refractive index profiles for axial thickness with fits to Eq. (3): (a) anterior axial without accommodation; (b) anterior axial with accommodation; (c) posterior axial without accommodation; (d) posterior axial with accommodation. The origin for the fits corresponds to the mid-point of the equatorial plane (the blue dot in Fig. 1). The fits are determined by combining all data, but the means and standard errors are determined from refractive index data at each normalized distance. The dashed lines are the 95% confidence limits of the fits.

Biomedical Optics EXPRESS

Figure 4 shows the refractive index profiles of the lens for the total axial dimension and for the equatorial direction for normalized equatorial distances, both without and with accommodation. With accommodation, the equatorial refractive index profiles become less steep at the periphery.

Figure 5 shows the refractive index profiles of the axial (anterior and posterior) and equatorial segments plotted against axial (anterior and posterior) and equatorial distances that are scaled by the mean axial (anterior and posterior) lens thickness and half the mean equatorial diameter, respectively.

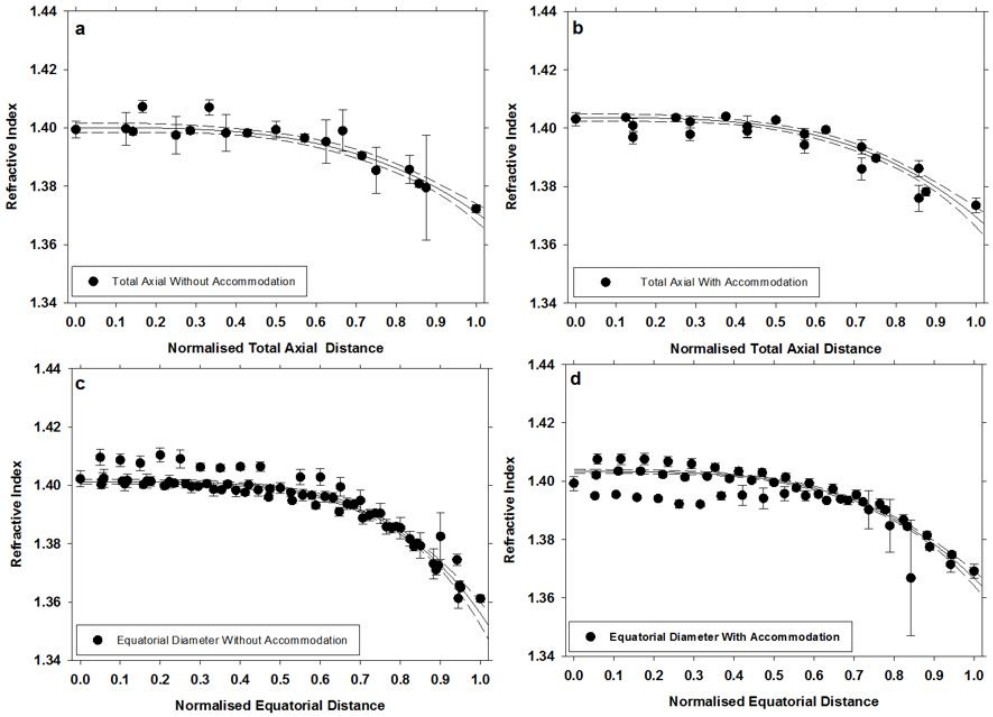

Fig. 4. Normalized refractive index profiles for the total axial and equatorial distances with fits to Eq. (3): (a), (c) without accommodation, and (b), (d) with accommodation. The origin for the axial profiles is the mid-point of the axis (red dot in Fig. 1) and that for the equatorial profiles is the mid-point of the equatorial plane (blue dot in Fig. 1). The fits are determined by combining all data and folding about the respective center points, but the means and standard errors are determined from refractive index data at each normalized distance. The dashed lines are the 95% confidence limits of the fits.

4. Discussion

In agreement with previous studies, we report that, with accommodation, lens thickness increases [2, 5–7, 10, 14–20], while lens equatorial diameter [5–7, 10, 14–17] and ciliary body ring diameter decrease [14–17, 21]. Table 4 is a summary of changes in lens thickness, lens diameter and ciliary ring diameter for our study and for previous in vivo studies using various methodologies, together with a recent in-vitro study [22]. These changes are given per diopter of accommodation, with some studies using the accommodation stimulus as the measure of accommodation, while others used estimates of accommodation response. It would be expected that the latter would give the larger, and more reasonable estimates, as accommodation response is less than stimulus, particularly as the ages of participants increase. For lens thickness, the in-vivo studies ranged from means of + 0.04 to + 0.08 mm/D with our study near the top (+ 0.08 ± 0.04 mm/D); despite using the stimulus method, this may be in part because all participants were young adults. For lens diameter, the nine in-vivo

Biomedical Optics EXPRESS

studies ranged from −0.05 to −0.14 mm/D with the majority of studies including ours having values of −0.07 to −0.08 mm/D. All but one in vivo study used MRI, with the Martinez-Enriquez et al. [6] study giving by far the greatest results; this might be a consequence of the method involving considerable shape modelling when being unable to image much of the lens through the iris. For ciliary ring diameter, the studies gave results in the range −0.07 to −0.11 mm/D, with our study continuing the finding in four out of five of the previous studies that reduction in ciliary ring diameter with accommodation was greater than the corresponding reduction in lens diameter.

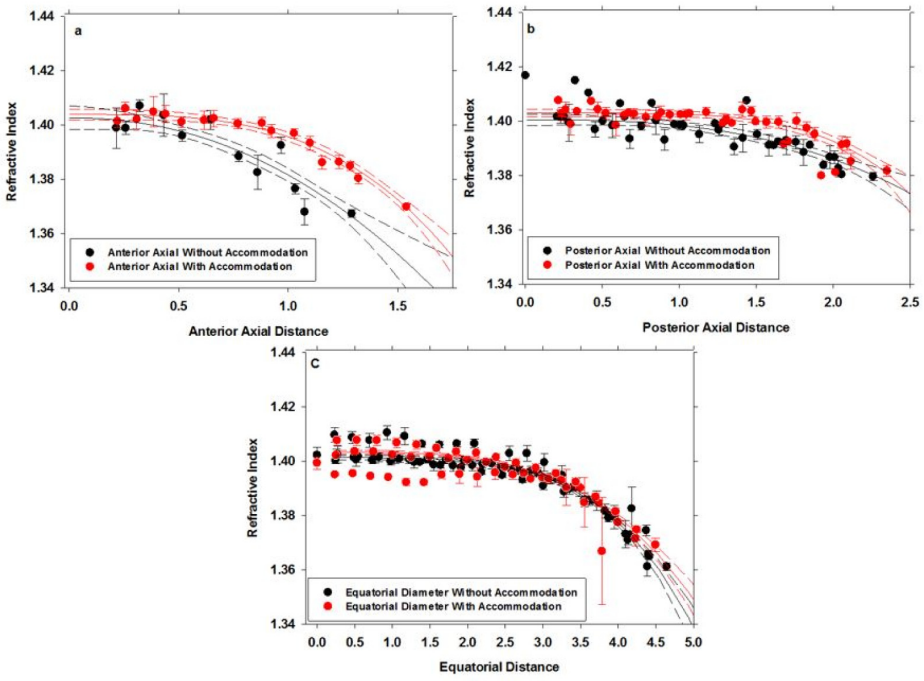

Fig. 5. Refractive index profiles, for distances (in mm) from the lens center, without and with accommodation: (a) anterior axial; (b) posterior axial; (c) equatorial. The fits are scaled from those in Figs. 3 and 4 by the mean thicknesses (axial and posterior axial) and half the mean diameter (equatorial) as given in Table 1. The fits are determined by combining all data, but the means and standard error are determined from refractive index data at each normalized distance. The dashed lines are the 95% confidence limits of the fits.

For the in-vitro study involving lens stretching and laser raytracing [22], the rate of change for lens thickness at + 0.07 mm/D was similar to in-vivo studies, the rate for lens diameter at −0.05 mm/D was at the low end of in-vivo studies, and ciliary ring diameter was much higher than in-vivo studies at 0.16 mm/D. As changes in lens power are about 30% greater than accommodation measured at the front of the eye [23], correction to make them more comparable with the in vivo studies using accommodation response would give respective rates of approximately 0.06, 0.08 and 0.19 mm/D.

An important finding of our study is the change in lens GRIN profiles with accommodation, with the anterior and posterior axial refractive index profiles becoming steeper at the periphery (Fig. 3) and the equatorial refractive index profiles becoming flatter at the periphery (Fig. 4). This is reflected in changes in p values for the corresponding power equation fits, with increases from 2.14 to 3.31 for the anterior axis and from 2.79 to 4.73 for the posterior axis (Table 2) and decrease for the equatorial axis from 4.34 to 3.66 (Table 3). The total axial profile does not show an obvious change in steepness with accommodation towards the periphery (Fig. 4). While none of the profiles are ideal for considering spatial

Biomedical Optics EXPRESS

variation in index, we think that taking into account the lens axial asymmetry is preferable to ignoring it as in the total axial profile approach in which center points of the axial profiles with/without accommodation correspond to considerably different regions in the lens.

Interestingly, the accommodated results have less scatter than the unaccommodated results relative to fitted curves (Fig. 3). We have no explanation as to why this occurred.

Table 4. Change in ocular parameters with accommodation from various in-vivo studies

Parameter	Study	Change (mm/diopter accommodation)*	Method, stimulus/response measure, comment
Axial thickness	This study	+ 0.08 ± 0.04	MRI, stimulus
	Strenk et al. [14]	+ 0.05 ± 0.03	MRI, stimulus, using ten participants 22-31 years
	Jones et al. [10]	+ 0.05 ± 0.02	MRI, stimulus
	Hermans et al. [7]	+ 0.06 ± 0.03	MRI, response
	Kasthurirangan et al. [15]	+ 0.05 ± 0.01	MRI, stimulus, ~6 D average
	Sheppard et al. [5]	+ 0.08 ± 0.04	MRI, response
	Richdale et al. [16]	+ 0.06	MRI, response
	Richdale et al. [17]	+ 0.06	MRI, response
	Richdale et al. [20]	+ 0.05 ± 0.02	AS-OCT, response
	Martinez-Enriquez et al. [6]	+ 0.07	AS-OCT, response
	Dubbelman et al. [2]	+ 0.05 ± 0.01	Scheimpflug stimulus
	Ni et al. [18]	+ 0.04 ± 0.01	Scheimpflug stimulus
	Ramasubramanian & Glasser [19]	+ 0.07	Ultrasound, stimulus
	Augusteyn et al. [22]	+ 0.07	In-vitro lens stretching, response, derived by combining equations from Figs. 4 and 5 of paper[#]
Lens diameter	This study	–0.07 ± 0.05	MRI, stimulus
	Strenk et al. [14]	–0.08 ± 0.02	MRI, stimulus, using ten participants 22-31 years
	Jones et al. [10]	–0.07 ± 0.03	MRI, stimulus
	Hermans et al. [7]	–0.07 ± 0.01	MRI, response
	Kasthurirangan et al. [15]	–0.05 ± 0.01	MRI, stimulus, ~6 D average
	Sheppard et al. [5]	–0.09 ± 0.07	MRI, response
	Richdale et al. [16]	–0.08	MRI, response
	Richdale et al. [17]	–0.08	MRI, response
	Martinez-Enriquez et al. [6]	–0.14	AS-OCT, response
	Augusteyn et al. [22]	–0.05	See [#] above
Ciliary body ring diameter	This study	–0.10 ± 0.07	MRI, stimulus
	Strenk et al. [14]	–0.10 ± 0.03	MRI, stimulus, using ten participants 22-31 years
	Strenk et al. [21]	–0.09	MRI, stimulus, using participants < 30 years
	Kasthurirangan et al. [15]	–0.07 ± 0.03	MRI, stimulus, ~6 D average
	Richdale et al. [16]	–0.11	MRI, response
	Richdale et al. [17]	–0.08	MRI, response
	Augusteyn et al. [22]	–0.16	See [#] above

*Some studies gave linear fits to data and standard deviations were not available

Biomedical Optics EXPRESS

Like us Kasthurirangan et al. [8] found similar changes in the decline in refractive index from center to the periphery along the equatorial diameter (*p* value changing from 6.30 ± 0.45 to 5.09 ± 0.28), but unlike us they found the axial refractive profiles become less steep at the periphery (4.90 ± 0.35 to 4.04 ± 0.24). The earlier study, which was carried out on an MRI system operating at 1.5T, used the total axial profile approach only and had poorer S/N and lower spatial resolution than the 3T data used in this study. Differences between the studies may also be due to a higher accommodation stimulus in the earlier study (between 6.9 and 4.8 D compared with a mean of 4.5 D in this study).

The current study has limitations. Firstly, accommodative response magnitude was not measured; about half the studies reported in Table 4 have this limitation, while the rest inferred response from refraction instruments at similar stimulus levels. Secondly as pointed out previously [8] "The data were inherently noisy due primarily to the limited sensitivity of the clinical MRI scanner for this type of measurement and the need to minimize scan times to reduce motion artifacts and avoid fatiguing the subject." With the growing availability of clinical MRI systems operating at higher magnetic fields of 7T and above, it should become possible to obtain high resolution refractive index profiles with good signal-to-noise ratio for individual lenses, similar to those that we have obtained ex-vivo [24], particularly with the advent of dedicated receiver coils for eye imaging at these fields.

5. Conclusion

We used magnetic resonance imaging to study ciliary body, lens dimensions and lens refractive index distributions in healthy young participants. With accommodation, ciliary body ring diameter and lens equatorial diameter decreased and lens thickness increased, with associated changes in refractive index profiles along axial and equatorial directions. This finding suggests that anatomically correct optical models of the crystalline lens would benefit from the changes in refractive index distribution that occur with accommodation e.g [25]. The geometrical parameters in Table 1 and power law fit parameters in Tables 2 and 3 may form a starting point for modeling such changes.

Acknowledgments

We thank the Centre for Advanced Imaging, University of Queensland, and in particular its radiographers Aiman Al Najjar and Anita Burns. This work was supported by Johnson & Johnson Vision.

Disclosures

The authors declare that there are no conflicts of interest related to this article.